Narrowband Emission and Enhanced Stability in Top-Emitting OLEDs with Dual Resonant Cavities

Wei He,[1,3] Qi Sun,[2] Zi-Yi Jin,[3,5] Hao-Feng Zheng,[6] Shuang-Qiao Sun,[3,5] Jun-Gui Zhou,[3] Shao-Cong Hou,[6] Yue-Min Xie,[3,4,*] Feiyu Kang[1], Guodan Wei[1,*] and Man-Keung Fung[2,3,5,*]

[1]Institute of Materials Research, Tsinghua Shenzhen International Graduate School, Tsinghua University, Shenzhen 518055, P. R. China

[2]Macao Institute of Materials Science and Engineering (MIMSE), MUST-SUDA Joint Research Center for Advanced Functional Materials, Zhuhai MUST Science and Technology Research Institute, Macau University of Science and Technology, Taipa 999078, Macau, China

[3]Institute of Functional Nano & Soft Materials (FUNSOM), Jiangsu Key Laboratory for Carbon-Based Functional Materials & Devices, Soochow University, 199 Ren'ai Road, Suzhou, 215123, Jiangsu, P. R. China

[4]Jiangsu Key Laboratory of Advanced Negative Carbon Technologies, Soochow University, Suzhou, 215123, Jiangsu, P. R. China

[5]Institute of Organic Optoelectronics, Jiangsu Industrial Technology Research Institute (JITRI), 1198 Fenhu Dadao, Wujiang, Suzhou 215200, P. R. China

[6]School of Electrical Engineering and Automation, Wuhan University, Wuhan, 430072 China

E-mail: ymxie@suda.edu.cn; weiguodan@sz.tsinghua.edu.cn;； mkfung@suda.edu.cn

Supplementary Note 1:

Preparation of Encapsulation Layers

SiNx films were prepared using Plasma Enhanced Chemical Vapor Deposition (PECVD) with flow rates of 20, 20, 40, and 200 standard cubic centimeters per minute (sccm) for silane (SiH_4), hydrogen (H_2), ammonia (NH_3), and nitrogen (N_2), respectively. The RF power was set to 200 W, and the chamber pressure was maintained at 1.4 Torr during deposition. The SiNx films were deposited at a temperature of 85 °C, achieving a thickness of approximately 1 μm with a deposition duration of 600 seconds.

Other layers, including LiF, were deposited using thermal evaporation, which is a well-established technique compatible with large-scale OLED manufacturing. This combination of PECVD and thermal evaporation ensures that the fabrication process remains scalable and integrates seamlessly with existing industry practices. Additionally, the SiN_x layer serves both as an optical component and as encapsulation, simplifying the overall production process.

Device fabrication

The high-reflectivity anode, composed of Indium Tin Oxide (ITO)/Ag/ITO, was deposited on a glass substrate by magnetron sputtering under a base vacuum of $1*10^{-3}$ Pa. ITO was prepared using Ar and O_2 gases at a DC power of 100 W and a sputtering pressure of 0.5 Pa, respectively. A 100-nm-thick Ag layer was prepared under Ar using an RF power of 200 W and a sputtering pressure of 2 Pa, respectively. Once the sandwich-type dielectric layer/metal layer/dielectric layer (DMD) structure was complete, the films were then annealed at 350℃ for 2 hours. Before device fabrication, the substrates were patterned by a picosecond laser, cleaned with ethanol for 15 minutes, dried in an oven at 100℃, and then treated with UV-ozone for 15 minutes. Subsequently, the substrates were transferred into a thermal evaporation

chamber (Suzhou Fangsheng FS-450) for OLED fabrication. 1,4,5,8,9,11-hexaazatriphenylene hexacarbonitrile (HAT-CN), 1,3,5-Triazo-2,4,6-triphos-phorine-2,2,4,4,6,6-tetrachloride (TAPC), tris(N-carbazolyl) triphenyl-amine (TCTA), 4,4′-bis(9-carbazolyl)-biphenyl (CBP), GD308, Bis(2-methyldibenzo[f,h]quinoxaline)(acetylacetonate) iridium(III)($Ir(MDQ)_2(acac)$), bis[(4,6-difluorophenyl)-pyridinato-N,C2']c(picolinate)iridium(III)(FIrpic) 4,6-bis[3,5-(dipyrid-4-yl)phenyl]-2-methylpyrimidine (B_4PYMPM) and 4,7-Diphenyl-1,10-phenanthroline (Bphen) were used to as the hole-injection layer, hole-transport layer, hole blocking layer, host, emissive dopants, electron-transport layer and electron-injection layer, respectively. The green device structure is HAT-CN (10 nm)/TAPC (x nm)/TCTA (10 nm) /CBP: 7vol% GD308 (20 nm)/B_4PYMPM (50 nm)/Bphen: 1 vol% Yb (10 nm)/Yb (1 nm)/Ag (23 nm); the red device structure is HAT-CN(10 nm)/TAPC(70 nm)/TCTA (10 nm) /CBP: 3vol% $Ir(MDQ)_2(acac)$(20 nm)/B_4PYMPM(50 nm)/Yb (1 nm)/Ag (23 nm); Blue device structure is HAT-CN(10 nm)/TAPC(110 nm)/TCTA(10 nm)/mCP: 12 vol% FIrpic (20 nm)/B_4PYMPM (50 nm)/Yb (1 nm)/Ag (23 nm).

The emission area of OLEDs is 10 mm^2. N,N'-bis(1-naphthyl)-N,N'-diphenyl-(1,1'-biphenyl)-4,4'-diamine(NPB) and Lithium fluoride (LiF) are all CPL materials used for top-emitting devices.

Measurement and characterization

The current density–voltage–luminance (J–V–L) characteristics, electroluminescence spectra, and efficiencies of the devices were measured by a Suzhou F-star Scientific Instrument. The reflectance of the cathode units was measured by Perkin Elmer Lambda 950 spectrophotometer in an integrating sphere. The refractive index, extinction coefficient, and film thickness of layers were measured by a J.A. Woollam Co., Inc. Alpha-SE ellipsometer with the angle of incidence at 70°.

Optical Simulation

All calculations of spectra and design parameters for dual microcavity top-emitting OLEDs (DMTEOLEDs) were conducted using MATLAB R2023b (MathWorks Inc., USA). The design parameters were calculated using the transfer matrix method. Simulations of far-field and dispersion relationships were conducted using the time-domain finite difference method (Lumerical FDTD Solutions, ANSYS Inc., USA). The refractive indices of materials used in simulations were determined using an ellipsometer. Perfect metal (-z direction) and perfect matching layer (otherwise: ±x, ±y, +z directions) were used as boundary conditions. A dipole light source was placed at the center of the emissive layer, and three individual simulations with different dipole orientations were conducted to mimic light generated in an isotropic emitter. To achieve real-time monitoring of energy emitted by the dipole, a cube monitor composed of six small two-dimensional energy monitors was employed to enclose it. The fraction of emitted power in air was calculated as the ratio between light power in the layer and dipole power. The far-field radiation map was calculated by averaging electric fields across three dipole orientations within a 2 μm region of the parallel interface. The dispersion relationship was analyzed based on data acquired from band-structure analysis group around the combined structure of CAV2 and ETL.

Supplementary Note 2:

The forward spectral emission intensity I(λ) from the optical cavity can be written as:

$$I(\lambda)=\frac{T_{top}\left[1+R_{bottom}+2\sqrt{R_{bottom}}\cos\left(\frac{4\pi nz}{\lambda}\right)\right]}{1+R_{bottom}R_{top}-2\sqrt{R_{bottom}R_{top}}\cos\left(\frac{4\pi nL}{\lambda}\right)}I_0(\lambda)=C(\lambda)I_0(\lambda) \quad (1)$$

where R_{top} (T_{top}) and R_{bottom} are the reflectivity (transmittance) of the top and bottom electrodes, respectively. λ, n and z are the wavelength, the refractive index and the distance from the emitter to the highly refractive anode, respectively. $I_0(\lambda)$ is the spectral emission intensity of the radiating emitter in the free space. In the Fabry-Perot cavity, the emission spectrum C(λ) is influenced by a combination of emitter, cavity length, and cavity characteristics. Specifically, the high reflectivity of the electrode (i.e., the mirror) determines the resonant characteristics of the cavity, which affects the shape of the emission spectrum. Therefore, changes in electrode reflectance can significantly affect the peak position and FWHM of the emission spectrum.

The microcavity gain factor formula is expressed as follows:

$$G_{cav}(\lambda)=\left[1-\frac{4\sqrt{R_{bottom}}\sin^2\left(\frac{\phi_{bottom}-2kz}{2}\right)}{\left(1+\sqrt{R_{bottom}}\right)^2}\right]\left[\frac{T_2\left(1+\sqrt{R_{bottom}}\right)^2}{\left(1+\sqrt{R_{bottom}R_{top}}\right)^2+4\sqrt{R_{bottom}R_{top}}\sin^2\left(\frac{\phi_{bottom}+\phi_{top}-2kL}{2}\right)}\right]\frac{\tau_{cav}}{\tau_0} \quad (2)$$

Where ϕ_{bottom} and ϕ_{top} is the phase shift of electrodes:

$$\phi=\tan^{-1}\left(\frac{2K_m n}{n^2-N_m{}^2-K_m{}^2}\right) \quad (3)$$

Here N_m and K_m are the refractive index of metal electrode.

According to the microcavity resonance formula,

$$\left|\phi_{bottom}\right|+\left|\phi_{top}\right|+\frac{2\pi}{\lambda}\sum 2n_i d_i = m\times 2\pi \quad (4)$$

we can obtain the relationship between the wavelength and viewing angle:

$$\lambda(\theta_{out})=\lambda(0)\sqrt{1-\left(sin\theta_{out}\sqrt{n}\right)^2} \quad (5)$$

Hence from formula (4), the longer the cavity length, the longer the peak wavelength. The formula (5) reveals that as the viewing angle increases, the peak wavelength is shifted towards the shorter wavelength.

$$FWHM=\frac{\lambda^2}{2L_{cav}}\times\frac{1-\sqrt{R_1R_2}}{\pi\sqrt[4]{R_1R_2}} \quad (6)$$

According to the FWHM formula (6), under the same cavity, the spectral narrowing is due to the reflectivity of cathode units.

The Fabry–Perot (FP) factor of 2nd resonant cavity is calculated as:

$$FP_{cav2}=\frac{n_{air}}{n_{cav2}}\times\frac{|t|^2}{\left[1+\left(|r_1||r_2|\right)^2-2\left(|r_1||r_2|\right)\cos\left(-\varphi_1-\varphi_2+2n_{cav2}L_{cav2}k_0\right)\right]} \quad (7)$$

Where $|r_1|$, $|r_2|$ and φ_1 φ_2 are the reflection magnitude and phase. $|t|$is the magnitude of the transmission coefficient at the interface of the SiN_x and the air.

Finally, the spectral characteristics of light extracted from CAV1 to the air can be designed based on a dual cavity gain (G_{CAV}) that is the product of G_{CAV1} and FP_{CAV2}.

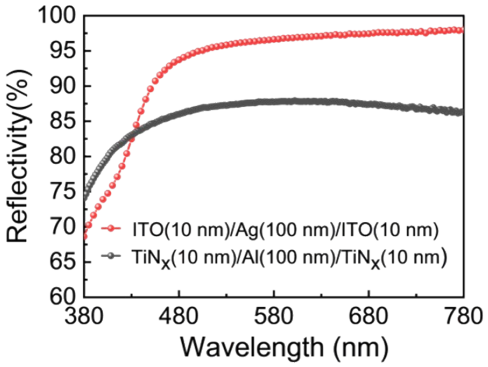

Figure S1 The experimental reflectivity spectra for ITO/Ag/ITO and ITO/Al/ITO anodes.

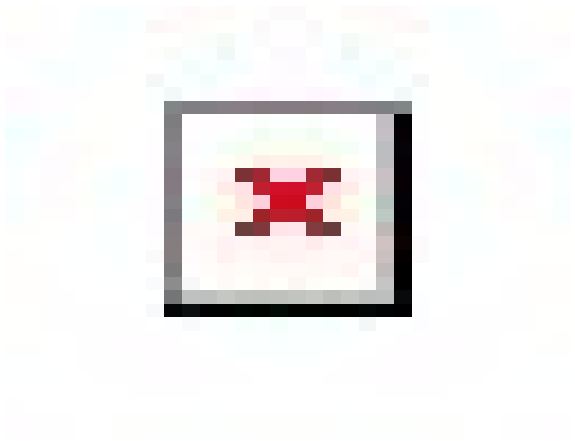

Figure S2 Outcoupling efficiency for different cavity lengths.

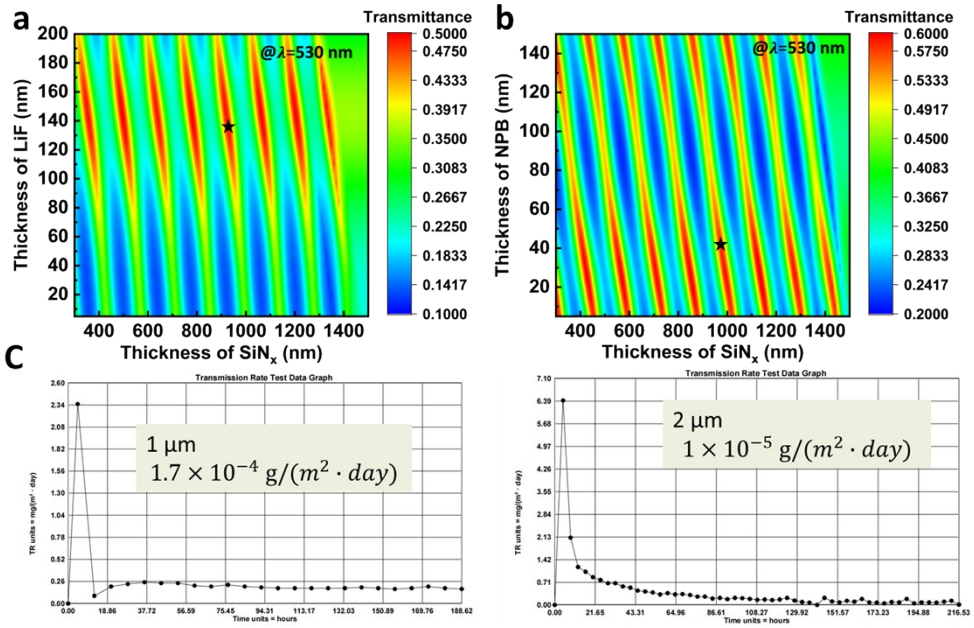

Figure S3 Simulated transmittance of 2nd resonant cavity (CAV2) with different thicknesses of the capping layer and SiN_x encapsulation layer at a peak wavelength of 530 nm. (a) LiF as the capping layer; (b) NPB as the capping layer; (c) water vapor transmission rates (WVTR) of different thickness of SiN_x.

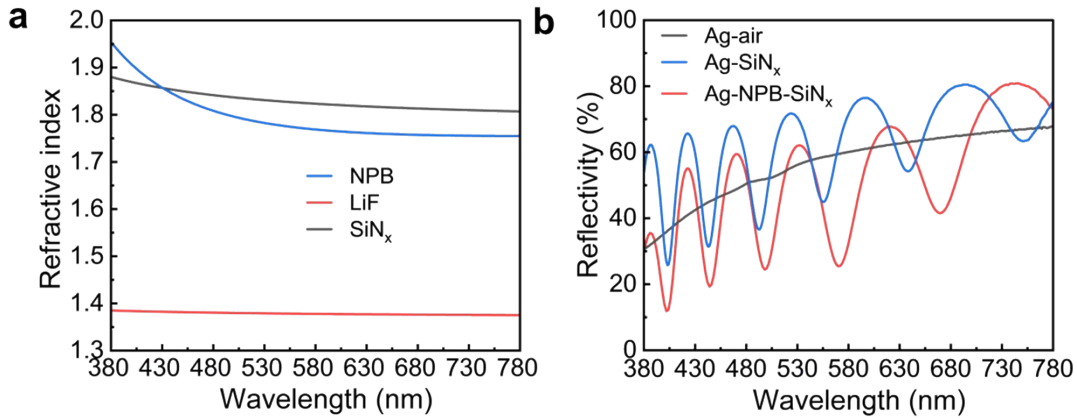

Figure S4 (a) Refractive index of SiN_x, NPB and LiF inside CAV2; (b) the interface reflectance of different CAV2.

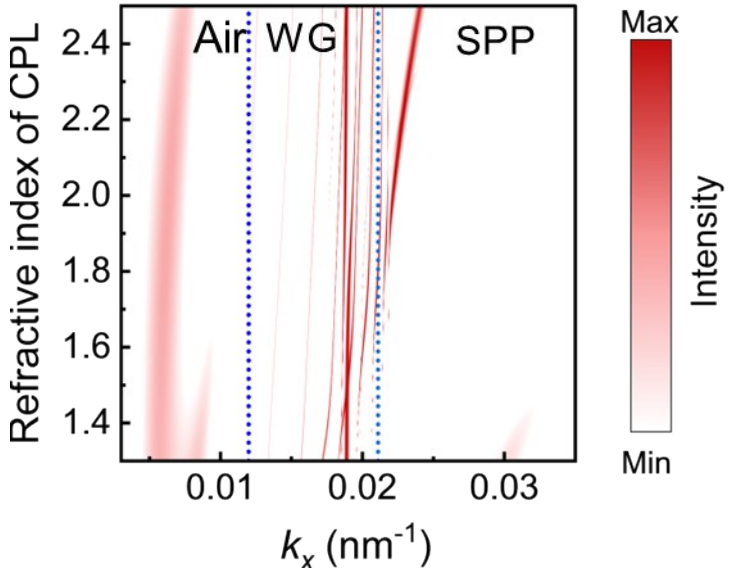

Figure S5 Power dissipation spectra as a function of refractive index of cathode capping layer when the 1st cavity length is 250 nm in dual microcavity top emitting OLED.

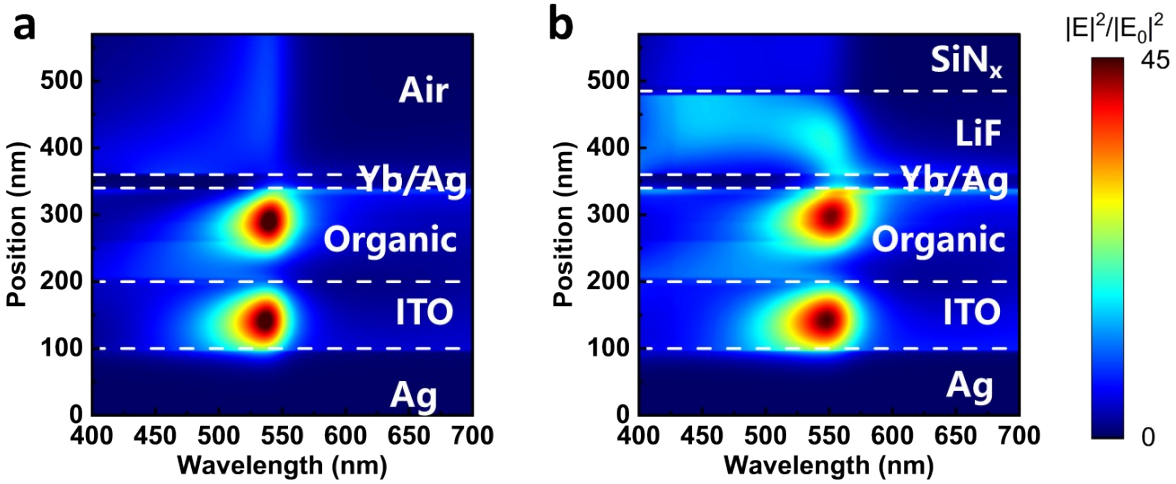

Figure S6 the Optical Intensity (E^2) in the x–z plane of TEOLEDs showing (a)control device;(b) the device with LiF/SiN_x.

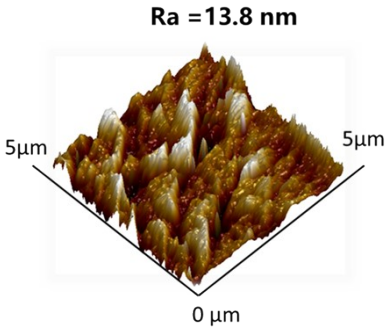

Figure S7 Surface roughness of SiN_x deposited on the LiF CPLs.

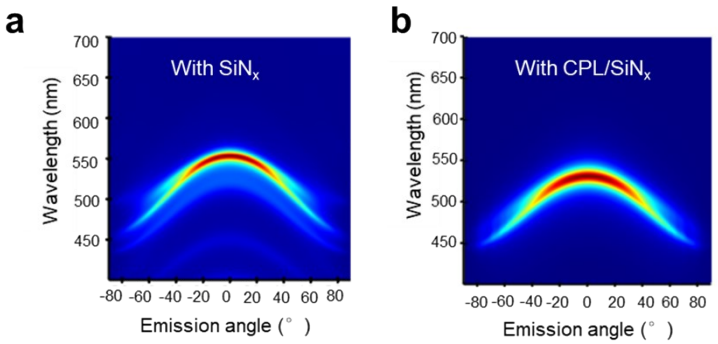

Figure S8 (a) the simulated far-field radiation contour of top-emitting device with SiN_x; (b) the simulated far-field radiation contour of top-emitting device with NPB/SiN_x.

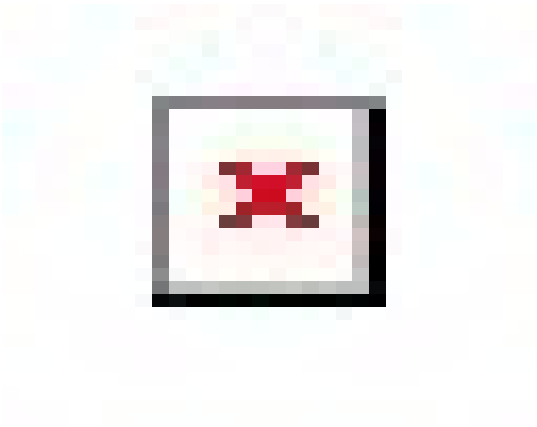

Figure S9 the angular EL spectrum for the device with LiF/SiN_x.

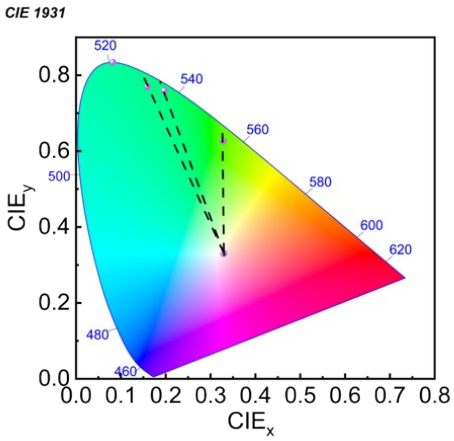

Figure S10 the method to calculate the color purity for the green device.

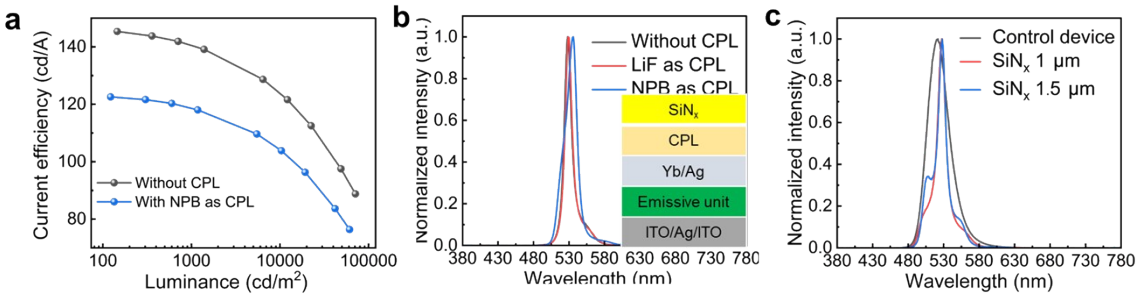

Figure S11 The devices with different CPL combinations. (a) the current efficiency of two combinations (b) Normalized EL spectra different capping layers; (c) Normalized EL spectra for SiN_x with different thicknesses.

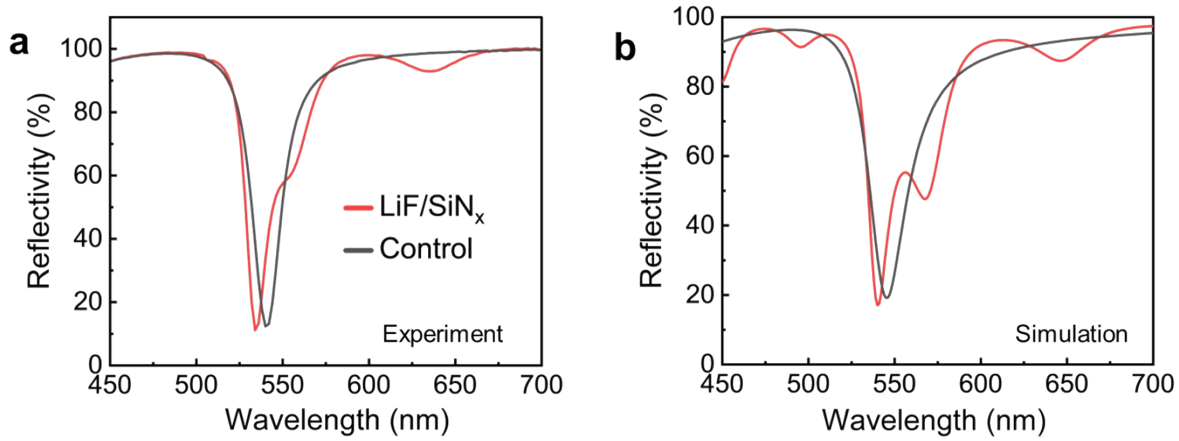

Figure S12 (a) the experimental reflectance of two types of green-emitting devices; (b) the simulated reflectance of two types of green-emitting devices.

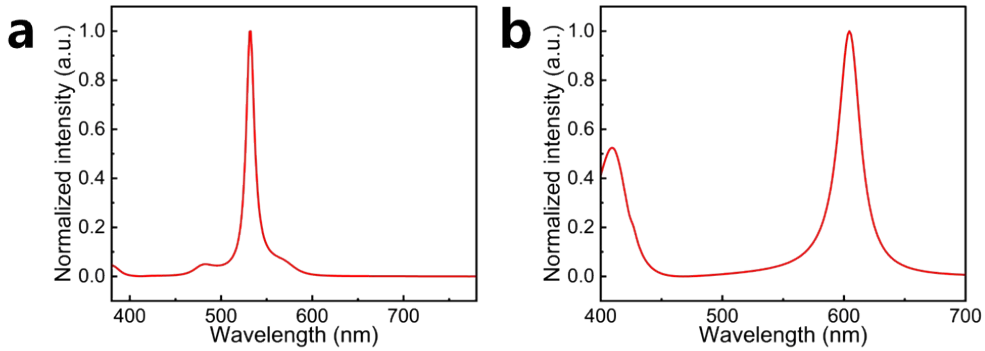

Figure S13 the calculated electroluminescence spectrum by FDTD: (a) green resonant cavity length; (b) the red resonant cavity length.

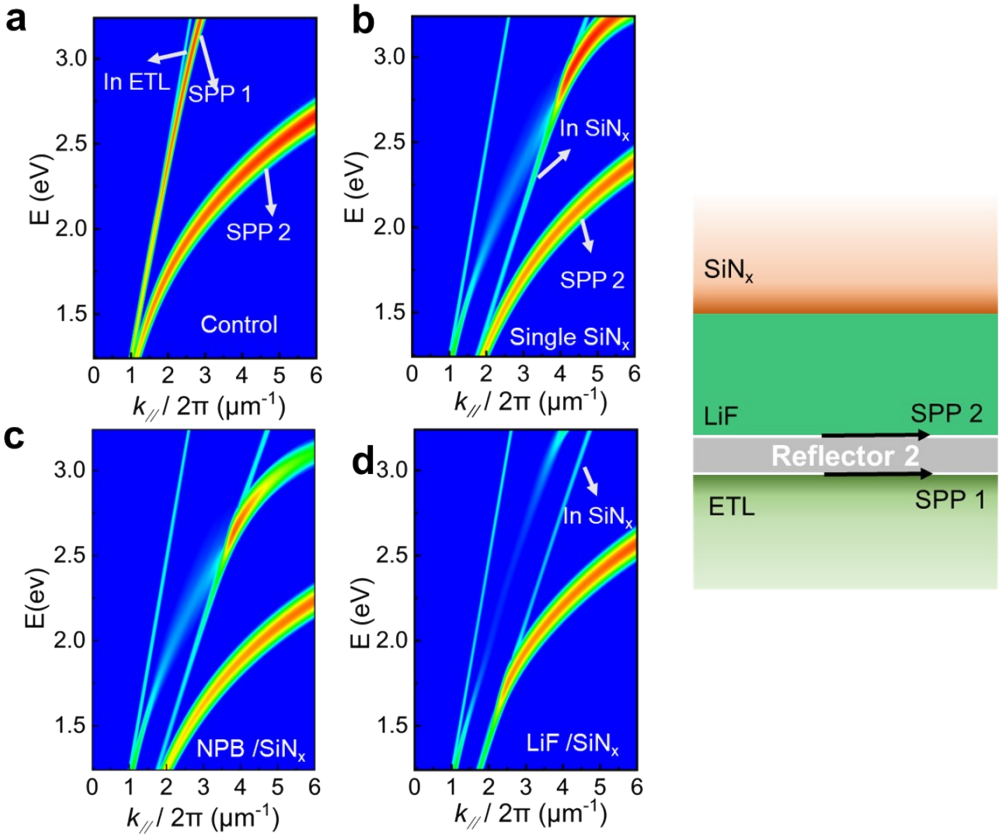

Figure S14 Dispersion relationship of different CAV2 for devices capped with (a) control structure (without any CPLs); (b) with single SiN_x; (c) 70 nm-thick NPB underneath SiN_x; (d) 120 nm LiF underneath SiN_x.

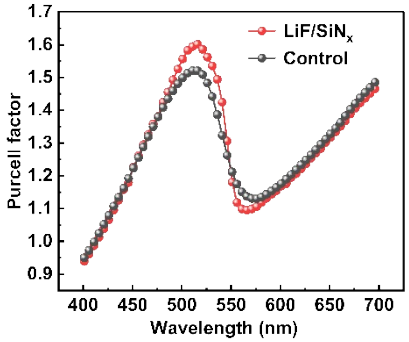

Figure S15 the caculated Purcell factor with or without LiF/SiN_x in green TEOLED.